Elastic strain around needle-shaped particles embedded in Al matrix

Joël Douin, P. Donnadieu, Florent Houdellier

Elastic strain around needle-shaped particles embedded in Al matrix

J. Douin [a,*], P. Donnadieu [b], F. Houdellier [a]

[a] CEMES – CNRS, 29 rue Jeanne Marvig, BP 94347, 31055 Toulouse cédex 04, France
[b] SIMAP, INP Grenoble – CNRS-UJF, BP 75, 38402 Saint Martin d'Hères cédex, France

Precise measurements of strain fields around precipitates embedded in a crystalline matrix were performed, and simple but accurate models were deduced from the observations. The measurements were carried out in an aged aluminum alloy containing needle-shaped particles. The displacement and strain fields around rod-shaped and lath-shaped particles were obtained from high-resolution electron micrographs using geometric phase analysis. The measurements reveal that strain field of a rod-shaped particle is well described by the classical Eshelby analytical elastic solution. For the more complex case of lath precipitates, it is shown that the strain field in the matrix can be simply approximated by a dislocations dipole. The methods developed are generally applicable to the characterization of strain in nano-structured materials, including those with complex or unknown structures.

Keywords: High-resolution electron microscopy; Nano-particles; Strain field modeling; Dislocation; Aluminum alloy

1. Introduction

Strain in crystalline matrices surrounding embedded nano-particles profoundly impacts the mechanical [1–3], magnetic [4], electronic [5] and/or optoelectronic [6–8] properties of composite materials. For example, strain may promote or prevent nucleation and/or growth of nano-particles and is instrumental for their auto-assembly [9], and the strain field around InAs islands is known to induce self-organization of quantum boxes [10]. Changes in electronic properties can also occur in silicon because of the shrinkage of the band gap induced by the strain field around SiC particles resulting from contamination [11]. Internal strain is also believed to induce dramatic changes for colossal magnetoresistance states in manganites containing ferromagnetic clusters [4]. The most classical example of the effect of nano-particles on matrix properties is precipitation hardening obtained by ageing treatment. It is a well-known solution for enhancing the mechanical properties [2], particularly for light metallic materials such as aluminum alloys, as the particles, or precipitates, oppose the motion of dislocations carrying the deformation, resulting in an increase in the yield strength of the material.

Among the precipitate characteristics controlling the mechanical properties, the residual strain field around the precipitate plays an essential role, as it changes the ability of motion of dislocations in the matrix in the vicinity of the precipitates [2,12–15]. The knowledge of the strain field produced by the inclusion of particles within the matrix is thus necessary to control the properties of precipitate-hardened materials. However, in many alloys, the hardening precipitation is produced by the decomposition of a supersaturated solid solution during heat treatment, depending on the solute content. As the decomposition of the supersaturated solid solution often leads to out of equilibrium metastable precipitates with complex structure and unknown composition, substantial efforts are necessary to characterize the structure of the precipitates in this type of material [3]. Moreover, this determination is highly dependent on and evolves with the exact composition and the annealing time and temperature. As a result, the strain field around particles within the matrix is difficult to model.

* Corresponding author. Tel.: +33 5 62 257873; fax: +33 5 62 257999.
E-mail addresses: joel.douin@cemes.fr, douin@cemes.fr (J. Douin).

The local strain fields outside the precipitates are caused by the mismatch of lattice parameters which exists between the coherent or semi-coherent precipitates and the matrix. When the strain is constant inside the precipitate, the strain outside can theoretically be reproduced by a continuous set of dislocations with infinitesimal Burgers vectors located at the interface between the matrix and the precipitate [16], but the determination of the distribution of the dislocations with infinitesimal Burgers vectors is quite complex. Using the equivalent inclusion method [17], the strain outside a precipitate, considered a disk-shaped particle, can also be theoretically determined, but it can usually only succeed for single ellipsoidal inclusion and for special conditions, such as for dilatational phase transformation strain [18], and is somewhat computationally intensive [19]. This theory can be extended to a distribution of inclusions [20], but still for a homogeneous elastic medium, i.e., the inclusions and the matrix have the same elastic constants. It is also possible to make the calculations assuming inhomogeneous elasticity [21,22], but in the present case such an approach may appear to be useless, as the structure of the precipitate is not known, and hence the elastic constants of the particle as well as its orientation relationship with the matrix.

It is the aim of this paper to show that strain fields in the matrix surrounding precipitates can be measured accurately using high-resolution transmission electron micrography (HRTEM) supplemented by image analysis. Such measurements are independent of the knowledge of the precipitates' crystallographic structures and give a clue to the modeling of their influence within the surrounding matrix. This study is exemplified in the case of needle-shaped precipitates in the T6-6056 Al alloy, and it is shown that the strain fields around precipitates can be simply modeled, depending on the shape of their cross sections.

2. Experimental

The commercially available 6056 alloy is an aluminum alloy with composition 0.86 wt.% Mg–0.92 wt.% Si–0.87 wt.% Cu–0.55 wt.% Mn–0.19 wt.% Fe. The material is first solutionized at 550 °C, then water quenched. The formation of the needle-shaped precipitates is promoted by T6 temper, which consists in keeping the alloy at 165 °C for 8 h. After such heat treatment, the microstructure is characterized by a high density of precipitates, in the order $\sim 10^{15}$–10^{17} particles cm^{-3}, usually showing two morphologies: needle-shaped particles with a roughly circular cross section (called rods), and needle-shaped particles with a transverse cross section close to a rectangle (called laths) [23–26]. Both rods and laths have their longest dimension along one of the $\langle 1\,0\,0 \rangle$ directions of the Al matrix. Their typical dimensions are: diameter ~5 nm and length ~50 nm for rods; width ~5 nm, thickness ~2 nm and length ~100 nm for laths.

HRTEM was used to image the atomic columns of the matrix in the close vicinity of the precipitates. The observations were performed on a Jeol 4000 EX instrument operating at 400 kV and equipped with a standard LaB_6 gun ($C_s = 1$ mm). Precipitates were observed end-on along their growth axis and particular care was taken to select precipitates emerging on both sides of the thin foil to avoid any relaxation effect in the plane of observation resulting from sample preparation: this was simply done by selecting precipitates showing no Moiré pattern resulting from the overlapping of the matrix and the precipitate. Notice also that such long particles, as they are usually longer than the thickness of the foil, usually emerge on both sides of the foil when the normal of the thin foil plane is close to the growth axis of the precipitates.

Image analysis was performed by geometrical phase analysis (GPA) [27] using a plug-in (HREM Research Inc. [28]) implemented in GATAN Digital Micrograph© Software. Owing to the low level of strain around the precipitates, the signal to noise ratio is usually quite low so the authors chose to use digital processing with a large spatial resolution ($\leqslant$2 nm) to smooth out the fluctuations resulting from imperfections in the image. This allows a smooth strain distribution in the matrix in the close vicinity of the precipitates to be obtained. For a 2-nm spatial resolution, the error, defined as the standard deviation of the measured strain in a $5 \times 5\ nm^2$ area [29], ranges from 0.1% to 0.2% (M. Hÿtch, private communication). Also, and as a general procedure, the reference area used in the digital processing as a strain-free area was chosen in the

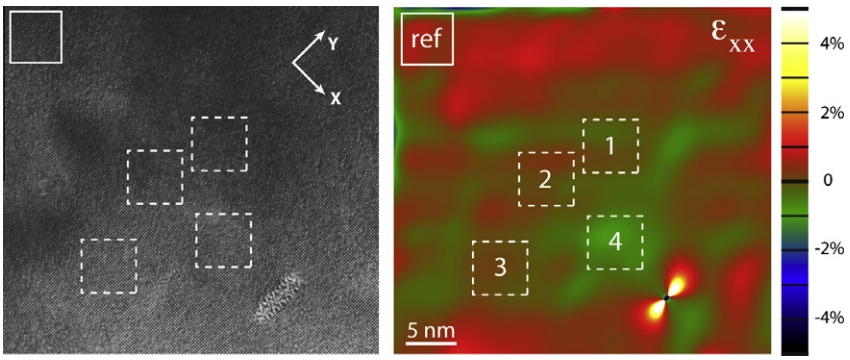

Fig. 1. Example of the determination of the mean value and standard deviation of strain ε_{xx} for the lath-shaped precipitate in Fig. 3. The values in the different areas are reported in Table 1. "Ref." corresponds to the area taken as the strain-free reference.

matrix as far as possible from the precipitate under study, as well as other strain sources, including other precipitates. On the images the standard deviation was never allowed to exceed 0.2%, which was then considered the maximum error on the measurements (see an example in Fig. 1 and Table 1). Notice finally that the projector lens of the TEM as well as the digitization of the negative introduce extra deformations in the image which could alter the accuracy of the results. To verify the validity of the measurements, it was also ensured that the measured strain dropped to zero when the measurements were performed far from the defects, in a perfect area of the crystal.

3. Measurements and modeling of the strain field around the precipitates

Figs. 2 and 3 show representative examples of the morphologies of precipitates in the Al-6056 alloy in the T6 state. Fig. 2a is an image of the aluminum matrix around a rod-shaped precipitate while Fig. 3a shows a lath-shaped precipitate, both precipitates being seen end-on along the [0 0 1] Al direction.

The determination of the crystallographic structure of the precipitates in such alloys is complex and may require a combination of through-focus exit-wavefunction reconstructions as well as HREM image calculation [3], which were not performed here. The lack of information on the precipitates structures implies that the misfit between the precipitates and the matrix as well as its elastic constants are not known, and prevents modeling of the strain field around the precipitate in a simple way. As exemplified in Ref. [12], a direct visual examination of the image does not allow the atomic displacements to be pointed out clearly when the precipitate is small and the misfit between the precipitate and its surrounding matrix is small. However, this difficulty can be overcome by direct measurement of the displacement field in the matrix using GPA [27]. GPA provides an accurate way to determine the displacement field $\boldsymbol{u}$ from HRTEM images, and has been used successfully to measure the strain field around precipitates in Si films, for example [30]. With GPA, no information can be simply extracted for the component of $\boldsymbol{u}$ parallel to the electron beam. However, as the stored energy resulting from the deformation ε_{zz} along the precipitate z-axis is roughly proportional to $L \cdot \varepsilon_{zz}^2$, where L is the length of the precipitate, a long precipitate is the signature of a low value of ε_{zz}. In other words, the strong preferential growth

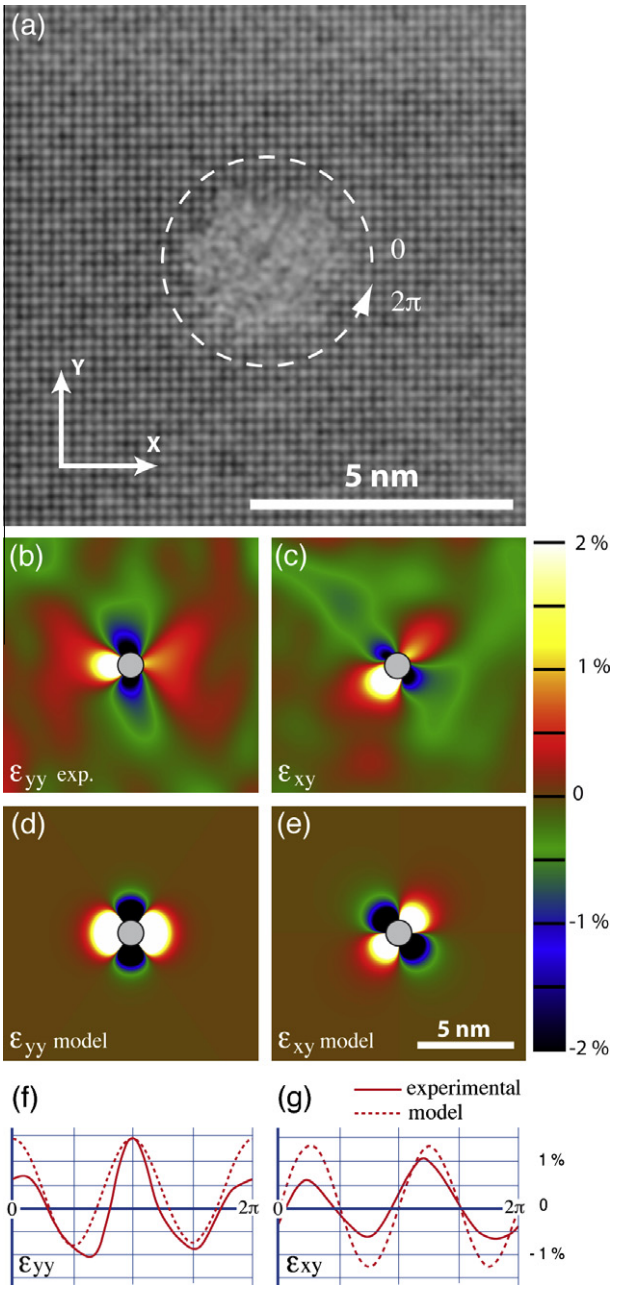

Fig. 2. Rod-shaped precipitate in the Al-6056-T6 alloy: (a) HRTEM image; the electron beam is the [0 0 1] direction of the Al matrix; (b) and (c) experimental strain ε_{yy} and ε_{xy}; (d) and (e) modeled ε_{yy} and ε_{yy} strain fields corresponding to an Eshelby inclusion with infinite size in the [0 0 1] viewing direction and a radial displacement field $u_r = -0.08r^{-2}$ fitted by comparing the experimental and modeled displacement fields; (f) and (g) line profiles of (d) and (e) at a constant distance (2 nm) from the symmetry center of the rod (along the dotted line in (a)).

Table 1
Mean values and standard deviation of the strain ε_{xx} measured in the areas defined in Fig. 1.

	Mean ε_{xx} (%)	Standard deviation of ε_{xx} (%)
Ref.	−0.0185	0.057
1	0.142	0.132
2	0.008	0.07
3	0.66	0.136
4	0.69	0.156

of the needle-shaped precipitates along the ⟨1 0 0⟩ axis attests that the residual strain ε_{zz} along their ⟨1 0 0⟩ growth direction is negligible compared with the other components of strain and will be neglected here. Notice, however, that for some particles with a less pronounced anisotropic shape, thus fully embedded in the matrix, it is possible to estimate the three-dimensional strain field by observing the same area in two different orientations [29].

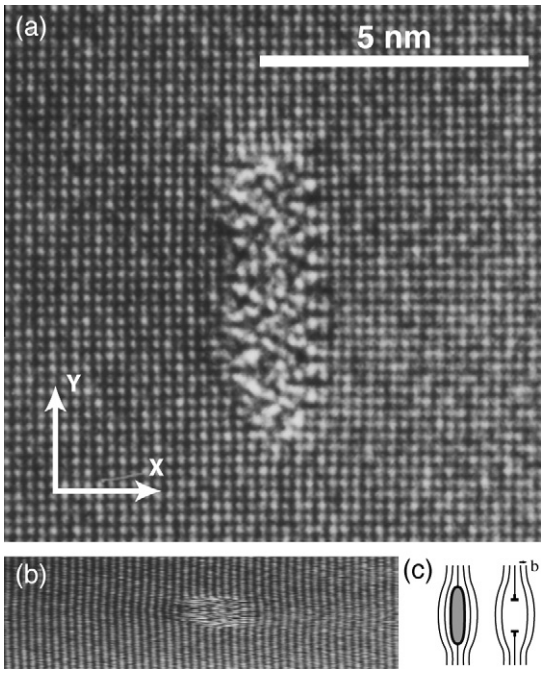

Fig. 3. Lath-shaped precipitate in the Al-6056-T6 alloy: (a) HRTEM image; the electron beam is the [0 0 1] direction of the Al matrix; (b) part of the same image but shrunk in the vertical direction to exemplify the distortion of the matrix parallel to the horizontal axis; (c) schematic of the horizontal displacements around a lath-shaped precipitate and around a dipole of edge dislocations.

3.1. Rod-shaped precipitate

Fig. 2b and c shows the experimental strains ε_{yy} and ε_{xy} in the matrix around the rod. For symmetry reasons, ε_{xx} is equivalent to ε_{yy} through a 90° rotation and is not presented here. Since the section of the rod-shaped precipitate in Fig. 2a is circular, an Eshelby-like elastic approach [31] can be tested to model the displacement field around the rod. The displacement field is supposed to be radial in the plane perpendicular to the rod axis, with an amplitude inversely proportional to the square of the distance r to the center of the precipitate: $u_r = k r^{-2}$. The strain field is then simply deduced by analytical derivation $\varepsilon_{ij} = 1/2(\partial u_i/\partial x_j + \partial u_j/\partial x_i)$. As k is a function of the unknown elastic properties of the precipitates, it cannot be determined a priori. By comparing the measured values of the displacement field with modeled ones, it is, however, possible to estimate k. Fig. 2d and e shows the modeled ε_{yy} and ε_{yy} strain fields corresponding to an Eshelby inclusion with infinite size in the [0 0 1] Al matrix direction and a radial displacement field $u_r = -0.08r^{-2}$. Fig. 2f and g depicts line profiles made at a constant distance from the symmetry center of the precipitate. These figures allow comparison of both the level of strain and the symmetry of the modeled and measured strain fields, and show good agreement. The model matches well both the distribution and intensity of the different components of the strain field around the rod-shaped precipitate, and this attests that the Eshelby elastic model is a good approximation for a rod-shaped precipitate at a nano-scale and near the surface of the particle. Of course, such a simple Eshelby model is not perfect, as it is based on a perfect cylindrical precipitate, which is not experimentally the case. In particular, the slight asymmetry of the measured strain can be related to a small change in the section of the precipitate along its axis.

3.2. Lath-shaped precipitate

Regarding the lath-shaped precipitates as in Fig. 3a, the situation is more complex. While the internal structure is still difficult to determine, the precipitate presents a preferential orientation relationship with the matrix, the lath facets being parallel to the {0 0 1} planes of the aluminum matrix. Fig. 4 shows the measured displacement fields in the horizontal (Fig. 4a) and vertical (Fig. 4b) ⟨1 0 0⟩ directions of the Al matrix around the precipitate in Fig. 3. The displacement field presents symmetry elements that attest that it is not radial as in the case of the rod. There is a ratio of ~4:1 between the amplitude of the displacements perpendicular (u_x) and parallel (u_y) to the longest dimension of the section of the precipitate. This is consistent with the general principle that the smaller the residual strain in the matrix in a direction, the easier the growth of the precipitate in this direction. In accordance, the aspect ratio of the precipitate section is 1:4.

To evidence the displacement field in the matrix due to the precipitate, a trick is to look at the image at a glancing angle or, equivalently, to shrink the image in the vertical direction. This makes the horizontal distortion of the matrix (Fig. 3b) more visible and gives a clue to the form of the displacement field around the precipitate. According to the sketch in Fig. 3c, the vicinity of the precipitate in the matrix has similarities with an assembly of dipoles of edge dislocations, and can be mimicked by the insertion of several (1 0 0) half planes, seven in the present case (Fig. 3c). In order to simplify the present description, the authors tried to model the precipitate by means of a single dipole of edge dislocations. As there is no shift between the (1 0 0) planes on both sides of the precipitate, the Burgers vector of the dislocations must be a perfect translation of the crystal in the plane of the image. Following Fig. 3c, the Burgers vectors of the dislocations were then chosen perpendicular to the (1 0 0) plane with a modulus equal to the periodicity of the crystal in this direction, i.e., $\vec{b} = \pm a/2[1\,0\,0]$, where a is the Al unit cell parameter. This description is sustained by the fact that, when the spatial resolution is large, the measured displacements artificially extend within the precipitate and the iso-values of the displacement fields converge to two symmetrical points (Fig. 4a). These two points are used as the locations of the two edge dislocations of the model dipole, and the corresponding displacement field is simply the sum of the displacements fields created by two edge dislocations. Since the Zener anisotropy factor of aluminum is close to 1, isotropic elasticity has been assumed. The only adjustable parameter for this modeling is the vertical separation distance between the dislocations, fixed here at 0.5 nm, which

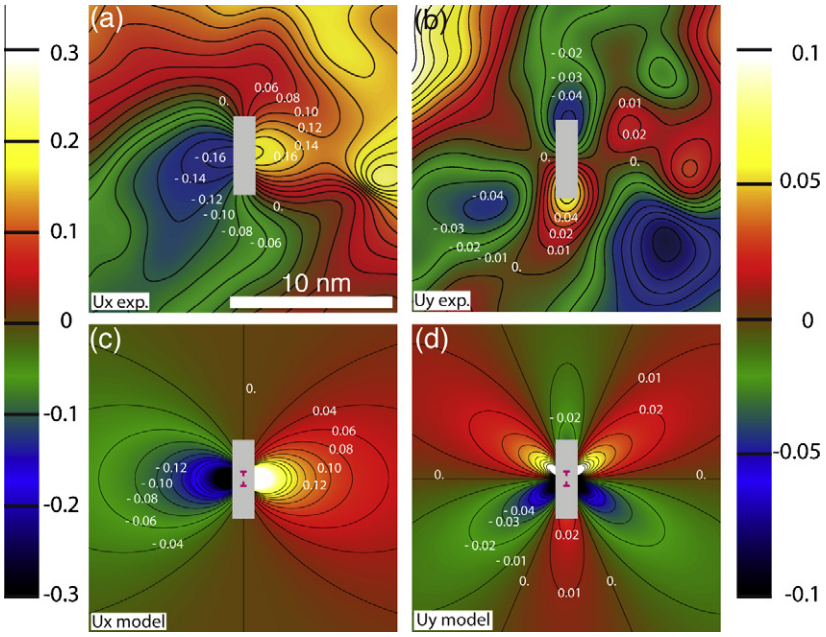

Fig. 4. Displacement fields around the lath in Fig. 3: (a) experimental displacements u_x in the horizontal direction; (b) u_y in the vertical direction; (c) and (d) the corresponding modeled fields components. For the measured and modeled displacement fields, u_x presents a diad symmetry (vertical mirror plane), while u_y shows a pseudo three-fold symmetry (vertical mirror plane and at $\pm 120°$).

is the distance between the two points where the iso-values of displacements converge in Fig. 4a.

While not perfect, the agreement with the displacements around the precipitate is relatively good for such a simplified model: the model essentially retains the symmetry elements as well as the level of intensities of the displacements. It is worth emphasizing that the GPA method involves reciprocal space filtering which cuts the high spatial frequencies and then reduces the resolution. In the present case, the mask is limiting the resolution to ~2 nm. It means that the phase fluctuations on a scale smaller than 2 nm are smoothed out. But the location of singularity points on the phase map is known with a precision much better than the resolution due to the mask. For instance, it was tested that, on the phase map of a dislocation, the point marking the dislocation core changes by ~0.1 nm when the mask varies from a size corresponding to 2 nm resolution to 0.7 nm resolution. Hence, the points that define the dipole of dislocations can be given by the GPA method with a precision higher than the 2 nm resolution, due to the mask.

However, the values of the phase (especially close to an interface) can show unreliable values for several reasons. At an interface, the phase values can be modified mainly by two effects: Fresnel diffraction and aberrations such as three-fold astigmatism [32]. In microscopes equipped with a C_s corrector, the lens effects are minimized owing to the numerous corrections provided by the system (three-fold astigmatism, coma, etc.). As images used in this work were being made with an uncorrected microscope, the profiles were taken at a safe distance. In addition, a strain field is meaningful to a certain extent and is expected to affect medium- or long-range distances, so testing the model at a few nanometers' distance is more relevant than at subnanometric distances.

Regarding the meaning of the distortion close to the precipitates, they are probably too sensitive to the effects mentioned above, and therefore comparison between phase values too close to the precipitate were discarded. The feature that survives perturbations due to the interface is actually the point of convergence of the displacement field, which is determined by symmetry and discontinuity of phase independent from the phase values. This is why a dipole distance of 0.5 nm can be derived from the phase map. This value is actually tested by comparison between the experimental strain field and modeling.

Finally, for differentiation of the displacement fields, it is possible to compute the related strain fields (Fig. 5). Again, as emphasized using line profiles at a constant distance from the symmetry center of the precipitate, the modeled strains fit well with the measured ones, in both the symmetry properties and the level of strain intensities. This shows that the strain field around a dislocation dipole is a good first approximation of the strain fields around a lath-shaped precipitate in the aluminum matrix.

4. Conclusion

It has been shown that it is possible to measure accurately the strain fields around needle-shaped nano-sized particles embedded in a crystalline matrix. From such measurements in an Al alloy, simple elastic modeling was proposed for both rod-shaped and lath-shaped precipitates. The agreement between measured strain fields and elastic descriptions of the strain in the matrix at the nanometer scale and near the precipitates' surface is striking, and can be accessed even if nothing is known about the structure and elastic properties of the particles themselves. For

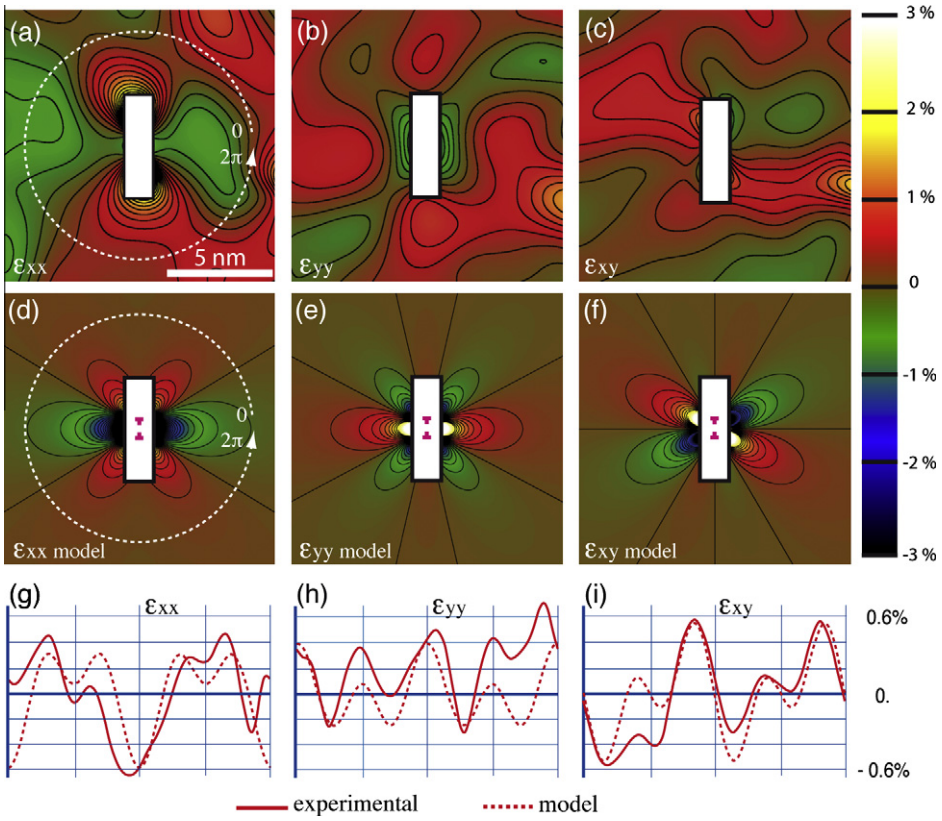

Fig. 5. Experimental and modeled strain fields around the lath-shaped nano-particle in Fig. 4: (a) ε_{xx}; (b) ε_{yy}; (c) ε_{xy}; (d)–(f) represent the modeled strain fields around a dipole of edge dislocations (iso-values every 0.2%); (g) and (h) the line profiles made at a constant distance (5.4 nm) from the symmetry center of the precipitate (along the dotted line in (a)).

rod-shaped precipitates, the classical Eshelby elastic model with cylindrical symmetry well describes the strain field around the precipitate, while small lath-shaped precipitates are very satisfactorily modeled by the elastic strain surrounding a dipole of dislocations.

The results demonstrate a method of providing a numerical description for the strain fields around needle-shaped precipitates, which can help in the study of other cases of nano-scaled inclusions embedded in a crystalline matrix. Having an analytical form for the displacement fields can be of great interest not only for simulating the mechanical behaviour through the interaction of dislocations with precipitates, but also for computing the residual stresses created by a dense assembly of organized nano-particles, known to tailor their optoelectronic properties, for example.

Finally and as far as mechanical properties are concerned, it is worth emphasizing that the level of residual strain is much higher around rod-shaped particles than around lath-shaped particles. Accordingly, it is expected that rods are stronger obstacles to the motion of dislocation than laths are.

Acknowledgement

This work was supported by the French National Research Agency (ANR) under Contract No. |0|6|-|B|L|A|N|-|0|2|0|5|.

References

[1] Taneka M, Abe F, Sawada K. Nature 2003;42:294.
[2] Nembach E. Particle strengthening of metals and alloys. Chichester: Wiley; 1996.
[3] Chen JH, Costan E, van Huis MA, Xu Q, Zandbergen HW. Science 2006;312:416.
[4] Dagotto E. Science 2005;306:257.
[5] Hÿtch MJ, Houdellier F, Hüe F, Snoeck E. Nature 2008;453:1086.
[6] Stangl J, Holý V, Bauer G. Rev Mod Phys 2004;76:725.
[7] Zhang X, Sharma P. Phys Rev B 2005;72:195345.
[8] Usami N, Ichitsubo T, Ujihara T, Takahashi T, Sazaki G, Nakajima K. J Appl Phys 2003;94:916.
[9] Shchukin VA, Bimberg D. Rev Mod Phys 1999;71:1125.
[10] Xie Q, Madhukar A, Chen P, Kobayashi N. Phys Rev Lett 1995;75:2542.
[11] Ujihara T, Yoshida Y, Lee WS, Takeda Y. Appl Phys Lett 2006;89:083110.
[12] Douin J, Donnadieu P, Epicier T, Dirras GF, Proult A, Silvain J-F. Mater Sci Eng A 2001;319–321:270.
[13] Dirras G, Donnadieu P, Douin J. Probl Mater Sci 2003;1:33.
[14] Donnadieu P, Dirras GF, Douin J. In: 8th Int conf on aluminium alloys, Mater Sci Forum, vol. 396–4; 2002. p. 1019.
[15] Arzt E. Acta Mater 1998;46:5611.
[16] Bollmann W. Acta Cryst A 1997;33:730.
[17] Mura T. Micromechanics of defects in solids. Dordrecht: Kluwer; 1987.
[18] Mori T, Cheng PC, Kato M, Mura T. Acta Metall 1978;26:1435.
[19] Gall K, Sehitoglu H, Chumiyakov YI, Kireeva IV, Maier HJ. J Eng Mater Technol 1999;121:19.
[20] Khachaturyan AJ. Theory of structural transformations in solids. Chichester: Wiley; 1983.

[21] Hu SY, Chen LQ. Acta Mater 2001;49:1879.
[22] Moulinec H, Suquet P. Physica B 2003;338:58.
[23] Matsuda K, Tada S, Ikeno S, Sato T, Kanio A. In: 4th Int conf aluminium alloys, vol. 1; 1994. p. 598.
[24] Edwards GA, Dunlop GL, Couper MJ. In: 4th Int conf aluminium alloys, vol. 1; 1994. p. 620.
[25] Donnadieu P, Carsughi F, Redjaïmia A, Diot C, Lapasset G. J Appl Cryst 1998;31:212.
[26] Delmas F, Casanove MJ, Lours P, Couret A, Coujou A. Mater Sci Eng A 2004;373:80.
[27] Hÿtch MJ, Snoeck E, Kilaas R. Ultramicroscopy 1998;74:131.
[28] http://www.hremresearch.com.
[29] Tirry W, Schryvers D. Nat Mater 2009;8:752.
[30] Chung J, Rabenberg L. Appl Phys Lett 2007;91:231902.
[31] Eshelby JD. Proc Roy Soc London 1957;241:376.
[32] Pénisson JM, Vystavel T. Ultramicroscopy 2002;90:163.